

**Electron doping evolution of the magnetic excitations in  $\text{BaFe}_{2-x}\text{Ni}_x\text{As}_2$** Huiqian Luo,<sup>1,\*</sup> Xingye Lu,<sup>1,\*</sup> Rui Zhang,<sup>1</sup> Meng Wang,<sup>1</sup> E. A. Goremychkin,<sup>2</sup> D. T. Adroja,<sup>2</sup> Sergey Danilkin,<sup>3</sup> Guochu Deng,<sup>3</sup> Zahra Yamani,<sup>4</sup> and Pengcheng Dai<sup>5,1,†</sup><sup>1</sup>*Beijing National Laboratory for Condensed Matter Physics, Institute of Physics, Chinese Academy of Sciences, Beijing 100190, China*<sup>2</sup>*ISIS Facility, Rutherford Appleton Laboratory, Chilton, Didcot, Oxfordshire OX11 0QX, United Kingdom*<sup>3</sup>*Bragg Institute, Australian Nuclear Science and Technology Organization, New Illawarra Road, Lucas Heights NSW-2234, Australia*<sup>4</sup>*Canadian Neutron Beam Centre, National Research Council, Chalk River Laboratories, Chalk River, Ontario K0J 1J0, Canada*<sup>5</sup>*Department of Physics and Astronomy, Rice University, Houston, Texas 77005, USA*

(Received 14 August 2013; revised manuscript received 6 October 2013; published 25 October 2013)

We use inelastic neutron scattering (INS) spectroscopy to study the magnetic excitations spectra throughout the Brillouin zone in electron-doped iron pnictide superconductors  $\text{BaFe}_{2-x}\text{Ni}_x\text{As}_2$  with  $x = 0.096, 0.15, 0.18$ . While the  $x = 0.096$  sample is near optimal superconductivity with  $T_c = 20$  K and has coexisting static incommensurate magnetic order, the  $x = 0.15, 0.18$  samples are electron overdoped with reduced  $T_c$  of 14 and 8 K, respectively, and have no static antiferromagnetic (AF) order. In previous INS work on undoped ( $x = 0$ ) and electron optimally doped ( $x = 0.1$ ) samples, the effect of electron doping was found to modify spin waves in the parent compound  $\text{BaFe}_2\text{As}_2$  below  $\sim 100$  meV and induce a neutron spin resonance at the commensurate AF ordering wave vector that couples with superconductivity. While the new data collected on the  $x = 0.096$  sample confirm the overall features of the earlier work, our careful temperature dependent study of the resonance reveals that the resonance suddenly changes its  $Q$  width below  $T_c$  similar to that of the optimally hole-doped iron pnictides  $\text{Ba}_{0.67}\text{K}_{0.33}\text{Fe}_2\text{As}_2$ . In addition, we establish the dispersion of the resonance and find it to change from commensurate to transversely incommensurate with increasing energy. Upon further electron doping to overdoped iron pnictides with  $x = 0.15$  and  $0.18$ , the resonance becomes weaker and transversely incommensurate at all energies, while spin excitations above  $\sim 100$  meV are still not much affected. Our absolute spin excitation intensity measurements throughout the Brillouin zone for  $x = 0.096, 0.15, 0.18$  confirm the notion that the low-energy spin excitation coupling with itinerant electron is important for superconductivity in these materials, even though the high-energy spin excitations are weakly doping dependent.

DOI: [10.1103/PhysRevB.88.144516](https://doi.org/10.1103/PhysRevB.88.144516)

PACS number(s): 74.25.Ha, 74.70.-b, 78.70.Nx

**I. INTRODUCTION**

Understanding the origin of superconductivity in strongly correlated electron materials is at the forefront of modern condensed matter physics.<sup>1,2</sup> Since high-transition temperature (high- $T_c$ ) superconductors such as copper oxides and iron pnictides are derived from electron or hole-doping to their antiferromagnetic (AF) order parent compounds,<sup>1,2</sup> much effort over the past 27 years has been focused on determining the role of short-range spin excitations in the superconductivity of these materials.<sup>3-5</sup> From inelastic neutron scattering (INS) experiments on copper oxide superconductors, it is well established that the low-energy ( $E \leq 100$  meV) spin excitations persist throughout the doping-induced superconductivity dome and vanish when superconductivity ceases to exist in the overdoped regime.<sup>3</sup> While INS failed to detect high-energy spin excitations near the AF ordering wave vector  $(0.5, 0.5)$  in overdoped copper oxides,<sup>3</sup> recent resonant inelastic x-ray scattering experiments find that high-energy ( $\geq 100$  meV) spin excitations in reciprocal space near the origin are almost independent of hole doping across the superconductivity dome.<sup>6,7</sup> In the case of iron pnictides (see Fig. 1),<sup>8-14</sup> INS experiments on single crystals of electron-doped  $\text{BaFe}_{2-x}\text{Ni}_x\text{As}_2$  (where  $T = \text{Co}, \text{Ni}$ ) have mapped out the doping evolution of the spin excitations.<sup>15-33</sup> In the undoped state,  $\text{BaFe}_2\text{As}_2$  exhibits nearly simultaneous tetragonal-to-orthorhombic lattice distortion and collinear AF order below  $T_N \approx 138$  K [see left inset of Fig. 1(a)].<sup>14</sup> In the AF ordered state,  $\text{BaFe}_2\text{As}_2$  forms randomly distributed orthorhombic twin domains rotated  $90^\circ$

apart. As a consequence, the low-energy spin waves from the two separate domains are centered around the AF ordering wave vectors  $\mathbf{Q}_{\text{AF}} = (\pm 1, 0)$  and  $(0, \pm 1)$ , respectively, in reciprocal space [see right inset in Fig. 1(a)]. INS experiments using time-of-flight (TOF) chopper spectrometer at the ISIS spallation neutron source in UK have measured spin waves of  $\text{BaFe}_2\text{As}_2$  in absolute units throughout the Brillouin zone and determined the spin-wave dispersions along the two high-symmetry directions as shown in the solid lines of Figs. 1(e) and 1(f).<sup>27</sup>

Figure 1(a) shows the schematic phase diagram of electron-doped  $\text{BaFe}_{2-x}\text{Ni}_x\text{As}_2$  as determined from transport and neutron diffraction experiments.<sup>34,35</sup> In previous work,<sup>30</sup> the evolution of the low-energy spin excitations was found to qualitatively follow the Fermi surface nesting picture and arise from quasiparticle excitations between the hole and electron Fermi pockets near  $\Gamma$  and  $M$  points, respectively.<sup>36-40</sup> By comparing spin waves of the parent compound with spin excitations of the optimally electron-doped superconductor  $\text{BaFe}_{1.9}\text{Ni}_{0.1}\text{As}_2$  in absolute units, it was found that electron doping on  $\text{BaFe}_2\text{As}_2$  affects only the low-energy spin excitations by broadening the spin waves below 80 meV and forming a low-energy ( $E_r \approx 7$  meV) neutron spin resonance below  $T_c$ , but has no impact on spin waves above 100 meV.<sup>29</sup> From systematic triple-axis INS<sup>28</sup> and nuclear magnetic resonance<sup>41</sup> measurements of the low-energy spin excitations in  $\text{BaFe}_{2-x}\text{Co}_x\text{As}_2$ , the suppression of superconductivity in electron-overdoped  $\text{BaFe}_{2-x}\text{Ni}_x\text{As}_2$  is found to be associated with vanishing low-energy spin excitations. Although these

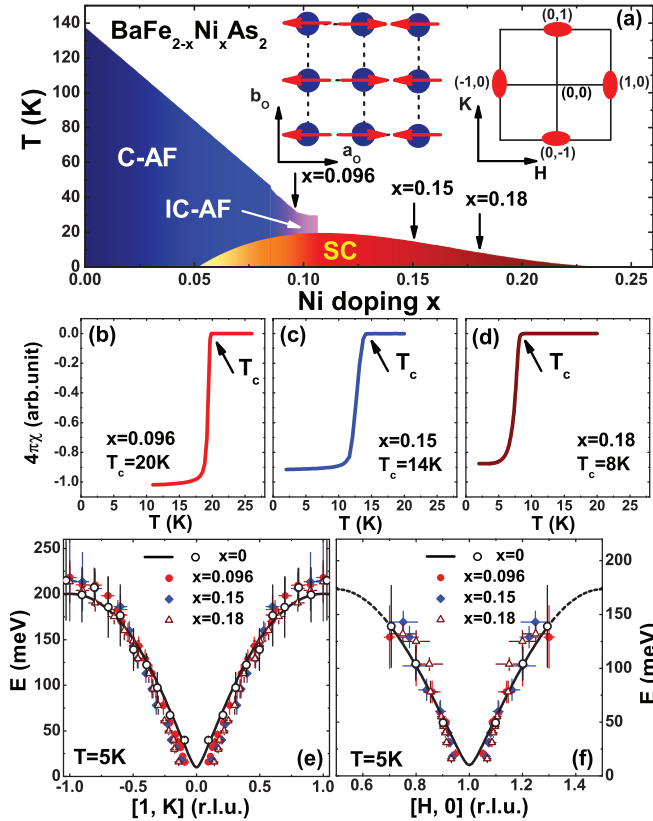


FIG. 1. (Color online) (a) The schematic electronic phase diagram of  $\text{BaFe}_{2-x}\text{Ni}_x\text{As}_2$ , where the arrows at  $x = 0.096, 0.15, 0.18$  indicate doping levels studied in this paper.<sup>34,35</sup> Inserts show the in-plane magnetic structure in real space and Brillouin zone in reciprocal space. (b)–(d) Direct current magnetic susceptibility indicates nearly 100% diamagnetic volume for all three measured dopings with  $T_c = 20, 14$ , and 8 K. (e) and (f) The dispersions of spin excitations along the  $[1, K]$  and  $[H, 0]$  directions for  $\text{BaFe}_{2-x}\text{Ni}_x\text{As}_2$  with  $x = 0.096, 0.15, 0.18$ . The solid and dash lines are spin wave dispersions in the parent compound  $\text{BaFe}_2\text{As}_2$  ( $x = 0$ ).<sup>27</sup>

results are consistent with the presence of a large spin gap ( $\sim 50$  meV) in the electron-overdoped nonsuperconducting  $\text{BaFe}_{1.7}\text{Ni}_{0.3}\text{As}_2$ ,<sup>33</sup> it is still unclear how spin excitations gradually evolve from optimally doped superconductor to electron-overdoped nonsuperconductor. Since spin excitations may mediate electron pairing for superconductivity,<sup>2</sup> it would be important to determine the temperature and electron-doping evolution of spin excitations in  $\text{BaFe}_{2-x}\text{Ni}_x\text{As}_2$  across the superconductivity dome [see Fig. 1(a)].

In this article, we report triple-axis and TOF INS studies of temperature and doping dependence of spin excitations in  $\text{BaFe}_{2-x}\text{Ni}_x\text{As}_2$ . For this work, we chose Ni-doping concentrations of  $x = 0.096, 0.15$ , and 0.18 with superconducting transition temperatures of  $T_c = 20$  K [Fig. 1(b)], 14 K [Fig. 1(c)], and 8 K [Fig. 1(d)], respectively. This range of Ni dopings covers the nearly optimally electron-doped to electron-overdoped iron pnictide superconductors, and complements the earlier work on the electron optimal  $x = 0.1$  superconductor<sup>29</sup> and the  $x = 0.3$  electron-overdoped nonsuperconductor.<sup>33</sup> Consistent with earlier work,<sup>22–24,29,30</sup> we find that the low-energy spin excitations in  $\text{BaFe}_{2-x}\text{Ni}_x\text{As}_2$  are transversely elongated

ellipses around the commensurate AF order wave vector. For the  $x = 0.096$  sample near optimal superconductivity, a neutron spin resonance appears at  $E_r = 7$  meV below  $T_c$ , and the mode forms transversely incommensurate spin excitations at higher energies. While the energy of the resonance is weakly temperature dependent, the transverse and radial widths of the mode show a superconductivity-induced narrowing below  $T_c$ . For samples at the overdoped side  $x = 0.15$ , superconductivity induces a transversely incommensurate resonance at  $E_r = 6.5$  meV. On increasing electron-doping further to  $x = 0.18$ , low-energy spin excitations have a broad commensurate component independent of superconductivity and a transversely incommensurate resonance below  $T_c$  at  $E_r = 5.5$  meV. By comparing TOF INS data in  $\text{BaFe}_{2-x}\text{Ni}_x\text{As}_2$  with  $x = 0.096, 0.15$ , and 0.18, we establish the wave vector and energy dependence of the spin excitations throughout the Brillouin zone from optimally electron-doped to electron overdoped iron pnictides. Our results are consistent with the idea that superconductivity in iron pnictides requires the low-energy spin excitation-itinerant electron interaction,<sup>33</sup> and indicate an intimate connection between spin excitations and superconductivity.

## II. EXPERIMENT

We carried out INS experiments using the MERLIN TOF chopper spectrometer at the Rutherford-Appleton Laboratory, UK. For the experiments, sizable single crystals of  $\text{BaFe}_{2-x}\text{Ni}_x\text{As}_2$  grown by self-flux method<sup>42</sup> were co-aligned on several aluminum plates by hydrogen-free glue with both in-plane and out-of-plane mosaic less than  $3^\circ$ . The total mass of our samples is 41 g for  $x = 0.096$ , 45 g for  $x = 0.15$ , and 25 g for  $x = 0.18$ , respectively. Using an orthorhombic crystalline lattice unit cell for easy comparison with the spin wave results of  $\text{BaFe}_2\text{As}_2$ ,<sup>27</sup> we define the wave vector  $\mathbf{Q}$  at  $(q_x, q_y, q_z)$  as  $(H, K, L) = (q_x a / 2\pi, q_y b / 2\pi, q_z c / 2\pi)$  reciprocal lattice units (r.l.u.), where  $a \approx b \approx 5.60$  Å, and  $c = 12.77$  Å. The samples are loaded inside a standard closed-cycle helium refrigerator with an incident beam parallel to the  $c$  axis. To probe spin excitations at different energies, we chose neutron incident beam energies of  $E_i = 20, 25, 30, 50, 80, 250, 450$  meV with corresponding Fermi chopper frequencies of  $\omega = 150, 200, 200, 400, 500, 550, 600$  Hz, respectively. To facilitate comparison with spin waves in  $\text{BaFe}_2\text{As}_2$ ,<sup>27,43</sup> spin excitations in doped materials are normalized to the absolute units (mbarn/sr/meV/f.u.) using a vanadium standard. The neutron scattering cross section  $S(\mathbf{Q}, E)$  is related to the imaginary part of the dynamic susceptibility  $\chi''(\mathbf{Q}, E)$  by correcting for the Bose population factor via  $S(\mathbf{Q}, E) = 1 / \{1 - \exp[-E / (k_B T)]\} \chi''(\mathbf{Q}, E)$ , where  $k_B$  is the Boltzmann's constant. We can then calculate the local dynamic susceptibility by using  $\chi''(E) = \int \chi''(\mathbf{Q}, E) d\mathbf{Q} / \int d\mathbf{Q}$  (in units of  $\mu_B^2/\text{eV}/\text{f.u.}$ ), where  $\chi''(\mathbf{Q}, E) = (1/3)\text{tr}[\chi''_{\alpha\beta}(\mathbf{Q}, E)]$ .<sup>22,29,33</sup>

In addition to the TOF INS measurements on MERLIN, we also took data on the  $x = 0.096$  compound using the TAIPAN thermal neutron triple-axis spectrometer at the Bragg Institute, Australian Nuclear Science and Technology Organization (ANSTO). The measurements were carried out on  $\sim 29$ -g co-aligned single crystals using the  $[H, 0, 3H] \times [0, -K, 0]$  scattering plane.<sup>34</sup> TAIPAN uses double focusing pyrolytic

graphite monochromator and vertical focusing analyzer with a pyrolytic graphite filter before the analyzer and a fixed final neutron energy of  $E_f = 14.87$  meV. In  $[H, K, 3H]$  scattering plane, we performed transverse scans along the  $[1, K, 3]$  direction for energies up to 25 meV. The  $\text{BaFe}_{2-x}\text{Ni}_x\text{As}_2$  samples with  $x = 0.096, 0.18$  for TOF and triple-axis experiments are aligned using a Photonic Sciences x-ray Laue camera and co-aligned by using TAIPAN triple-axis spectrometer at ANSTO and ALF crystal alignment facility at ISIS. The  $\text{BaFe}_{1.85}\text{Ni}_{0.15}\text{As}_2$  samples for TOF experiments are co-aligned using E3 neutron four-circle diffraction spectrometer at Canadian Neutron Beam Center in Chalk River, Canada.

### III. RESULTS

We first describe the evolution of spin excitation dispersions in  $\text{BaFe}_{2-x}\text{Ni}_x\text{As}_2$ . Figures 1(e) and 1(f) show the overall dispersions along the  $Q = [1, K]$  and  $[H, 0]$  directions for  $x = 0.096, 0.15$  and  $0.18$  compared with the parent compound  $x = 0$  (black solid lines). While the spin excitations at low-energy below  $\sim 100$  meV become slightly more dispersive upon Ni doping, the high-energy spin excitations are not much affected by electron doping, similar to those in the heavily

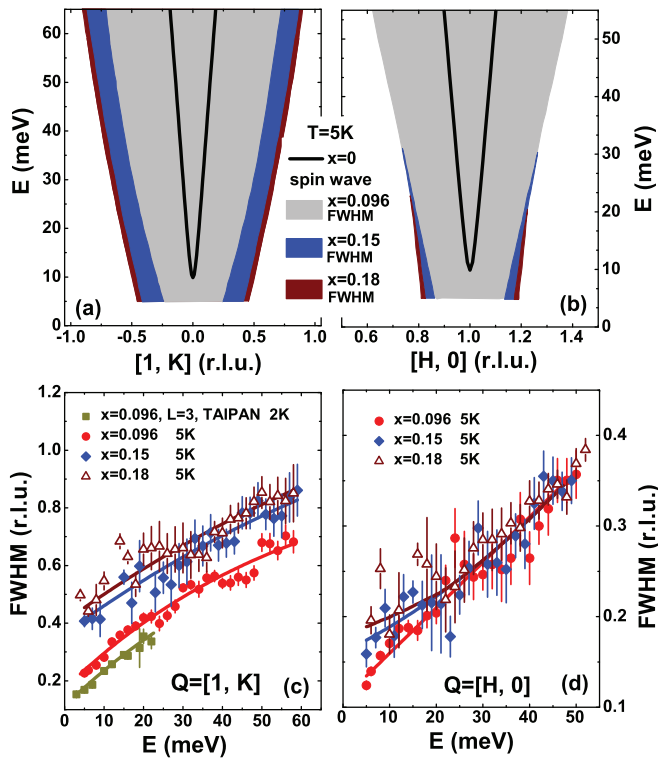


FIG. 2. (Color online) Comparison of the dispersions of low-energy spin waves in  $\text{BaFe}_2\text{As}_2$  with the FWHM of spin excitations in  $\text{BaFe}_{2-x}\text{Ni}_x\text{As}_2$  with  $x = 0.096, 0.15, 0.18$  along the  $[1, K]$  and  $[H, 0]$  directions. (a) and (b) The solid lines show spin wave dispersions of  $\text{BaFe}_2\text{As}_2$ .<sup>27</sup> The gray, blue, and brown regions show the FWHM of low-energy spin excitations of  $\text{BaFe}_{2-x}\text{Ni}_x\text{As}_2$  with  $x = 0.096, 0.15, 0.18$  along the  $[1, K]$  and  $[H, 0]$  directions, respectively. (c) and (d) Energy dependence of the FWHM along the transverse  $[1, K]$  and longitudinal  $[H, 0]$  directions as determined from TOF INS measurements. The FWHM of peak along the  $[1, K, 3]$  direction from the triple-axis experiments is also shown in (c).

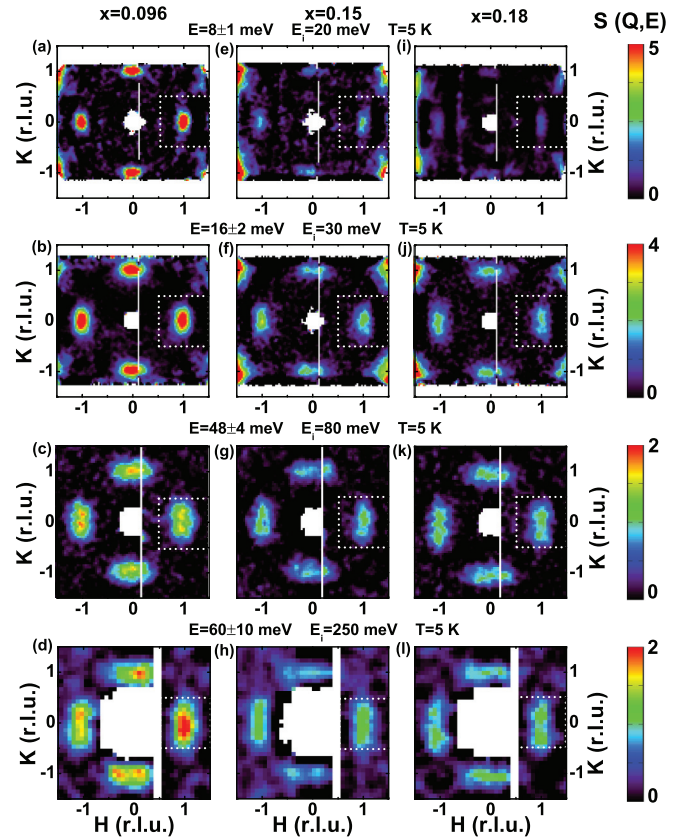


FIG. 3. (Color online) Comparison of two dimensional constant-energy slices through the magnetic excitations of  $\text{BaFe}_{2-x}\text{Ni}_x\text{As}_2$  ( $x = 0.096, 0.15$  and  $0.18$ ) at energies of (a),(e),(i)  $E = 8 \pm 1$ , (b),(f),(j)  $16 \pm 2$ , (c),(g),(k)  $48 \pm 4$ , and (d),(h),(l)  $60 \pm 10$  meV. The data in (a),(e),(i), (b),(f),(j), (c),(g),(k), and (d),(h),(l) are collected using  $E_i = 20, 30, 80, 250$  meV, respectively. For  $E_i \leq 80$  meV, images are obtained after subtracting a radially symmetric  $Q$ -dependent background integrated from the diagonal line of the entire zone  $-2 < H < 2$  and  $-2 < K < 2$ , which is mainly from the phonon scattering of the aluminum sample holders. For  $E_i \geq 250$  meV, images are obtained after subtracting the background integrated from  $1.8 < H < 2.2$  and  $-0.2 < K < 0.2$ . The color bars represent the vanadium normalized absolute spin excitation intensity in the units of mbarn/sr/meV/f.u. and the dashed boxes indicate AF zone boundaries for a single FeAs layer.

electron overdoped  $\text{BaFe}_{1.7}\text{Ni}_{0.3}\text{As}_2$ . These results suggest that the effective magnetic exchange couplings  $J$  are not much affected by electron-doping in  $\text{BaFe}_{2-x}\text{Ni}_x\text{As}_2$  for  $x \leq 0.3$ .<sup>33</sup>

To further study the effect of electron-doping to the low-energy ( $E < 60$  meV) spin excitations, we fit the wave-vector dependence of the spin excitations along the  $[1, K]$  and  $[H, 0]$  directions by Gaussian on a linear background to estimate their full-width-at-half-maximum (FWHM) in  $\text{BaFe}_{2-x}\text{Ni}_x\text{As}_2$  with  $x = 0.096, 0.15, 0.18$ . For comparison, we also probe the low-energy spin excitations on  $\text{BaFe}_{2-x}\text{Ni}_x\text{As}_2$  with  $x = 0.096$  using TAIPAN triple-axis spectrometer along the  $Q = [1, K, 3]$  direction. The solid black lines in Figs. 2(a) and 2(b) are spin wave dispersions of  $\text{BaFe}_2\text{As}_2$  estimated using the previous obtained in-plane effective magnetic exchange couplings<sup>27</sup> and appropriate spin anisotropy gap values.<sup>44</sup> The shaped area in Figs. 2(a) and 2(b)

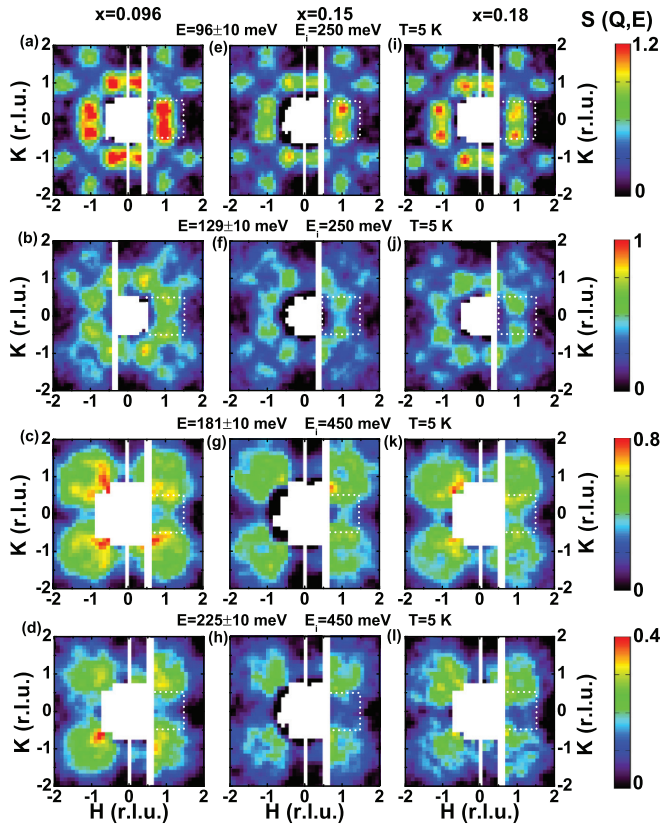


FIG. 4. (Color online) Two-dimensional constant-energy slices through the magnetic excitations of  $\text{BaFe}_{2-x}\text{Ni}_x\text{As}_2$  ( $x = 0.096, 0.15$  and  $0.18$ ) at energies of (a),(e),(i)  $E = 96 \pm 10$ , (b),(f),(j)  $129 \pm 10$ , (c),(g),(k)  $181 \pm 10$ , and (d),(h),(l)  $225 \pm 10$  meV obtained with  $E_i = 250$  and  $450$  meV along the  $c$  axis.

show the FWHM of spin excitations for  $\text{BaFe}_{2-x}\text{Ni}_x\text{As}_2$  with  $x = 0.096, 0.15, 0.18$  along the  $[1, K]$  and  $[H, 0]$  directions, respectively. Figure 2(c) shows energy dependence of the spin excitation widths along the  $[1, K]$  direction. Within the probed energy range ( $3 \leq E \leq 60$  meV), the widths of spin excitations increase monotonically with increasing energy and the electron-doping level  $x$  for these three samples. For  $\text{BaFe}_{1.904}\text{Ni}_{0.096}\text{As}_2$ , the spin excitation widths determined from the triple-axis experiments are slightly smaller than that from the TOF measurements due to the differences in the instrumental resolutions in these two techniques. Figure 2(d) shows the energy dependence of the spin excitation widths along the  $[H, 0]$  direction, which are almost independent of electron doping above 30 meV. Thus the low-energy spin excitations are transversely elongated upon doping and become broader than spin waves in the undoped compound.

To directly compare the evolution of spin excitations as a function of increasing electron-doping  $x$ , we show in Figs. 3 and 4 TOF INS measurements for  $x = 0.096, 0.15, 0.18$  obtained on MERLIN using identical setup. The scattering intensity is normalized to absolute units of mbarn/sr/meV/f.u. using a vanadium standard and the dashed boxes mark the AF Brillouin zone for the magnetic unit cell with single  $\text{Fe}^{2+}$ . For energies below 70 meV [ $E = 8 \pm 1$  meV, Figs. 3(a), 3(e), 3(i);  $16 \pm 2$  meV, Figs. 3(b), 3(f), 3(j);  $48 \pm 4$  meV, Figs. 3(c), 3(g), 3(k);  $60 \pm 10$  meV, Figs. 3(d), 3(h), 3(l) for  $x = 0.096, 0.15,$

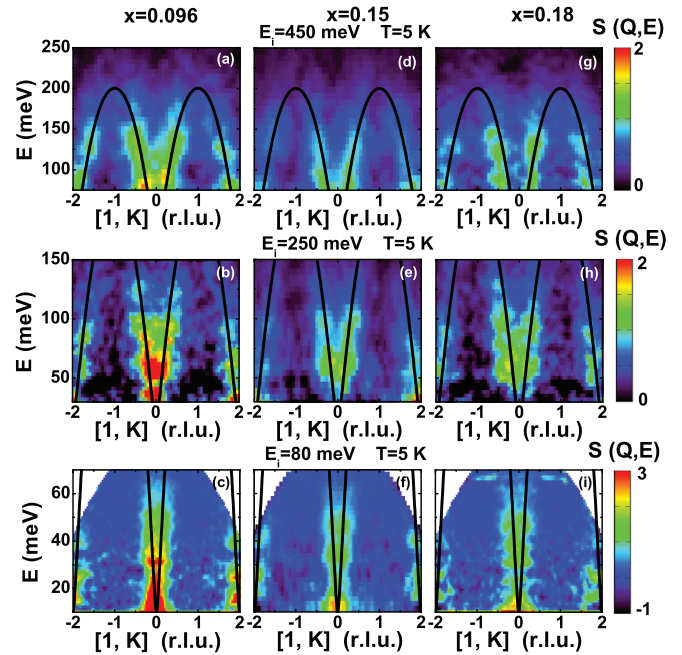


FIG. 5. (Color online) Energy dependence of the two-dimensional slices along the  $Q = [1, K]$  direction with  $E_i = 80, 250,$  and  $450$  meV for panels (c),(f),(i), (b),(e),(h), and (a),(d),(g), respectively. The solid lines are dispersions of spin waves in  $\text{BaFe}_2\text{As}_2$ .<sup>27</sup>

and  $0.18$ , respectively], spin excitations are transversely elongated ellipses centered around the in-plane AF ordering wave vectors  $\mathbf{Q}_{\text{AF}} = (\pm 1, 0)$  and  $(0, \pm 1)$  due to the two twinned domains. The excitations become more transversely elongated and decrease in intensity with increasing  $x$ . On increasing energies to  $E = 96 \pm 10$  meV [Figs. 4(a), 4(e), and 4(i) for  $x = 0.096, 0.15,$  and  $0.18$ , respectively], spin excitations start to split transversely away from the AF ordering wave vectors and become less doping dependent. For energies  $E = 129 \pm 10$  meV [Figs. 4(b), 4(f), and 4(j)],  $E = 181 \pm 10$  meV [Figs. 4(c), 4(g), and 4(k)], and  $E = 225 \pm 10$  meV [Figs. 4(d), 4(h), and 4(l)], spin excitations become rather similar, and are almost electron-doping independent.

Figure 5 compares the background subtracted scattering for the  $E_i = 450, 250,$  and  $80$  meV data projected in the wave vector ( $Q = [1, K]$ ) and energy space for  $\text{BaFe}_{2-x}\text{Ni}_x\text{As}_2$  with  $x = 0.096, 0.15,$  and  $0.18$ . These incident beam energies were chosen to probe spin excitations at different energies. Figures 5(a), 5(d), and 5(g) show the  $E_i = 450$  meV data for the  $x = 0.096, 0.15,$  and  $0.18$  samples, respectively. Similar data with  $E_i = 250$  and  $80$  meV are shown in Figs. 5(b), 5(e), 5(h), and 5(c), 5(f), 5(j), where the solid lines are spin wave dispersions for  $\text{BaFe}_2\text{As}_2$ .<sup>27</sup> While magnetic scattering clearly decreases with increasing doping at energies below 60 meV, they are virtually unchanged for energies above 100 meV, consistent with results in Figs. 3 and 4. To quantitatively determine the evolution of spin excitations for  $\text{BaFe}_{2-x}\text{Ni}_x\text{As}_2$  with  $x = 0, 0.096, 0.15,$  and  $0.18$ , we show in Figs. 6 and 7 constant-energy cuts at different energies along the  $[1, K]$  and  $[H, 0]$  directions, respectively. At  $E = 5 \pm 1$  [Fig. 6(a)] and  $8 \pm 1$  meV [Fig. 6(b)], the commensurate spin excitations at  $x = 0.096$  become weaker and transversely

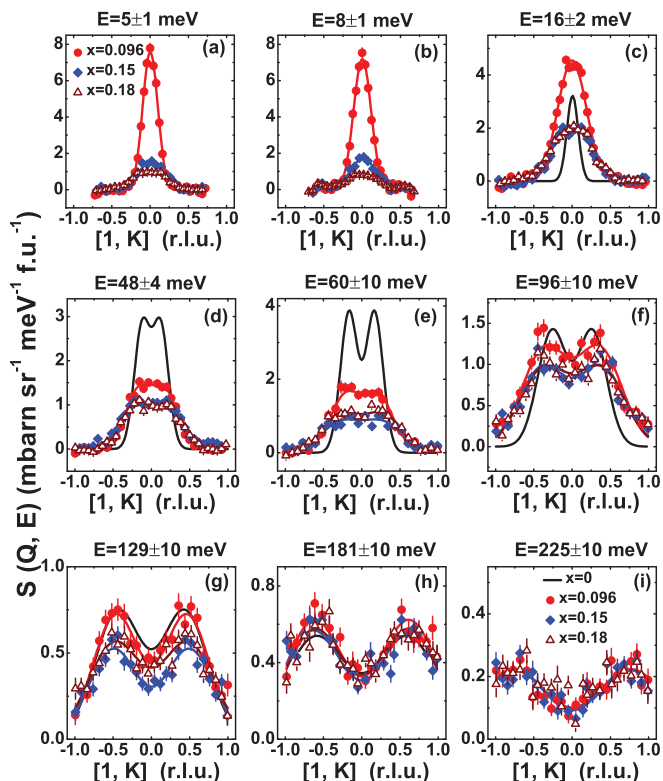


FIG. 6. (Color online) Constant-energy cuts in the spin excitations of  $\text{BaFe}_{2-x}\text{Ni}_x\text{As}_2$  along the  $[1, K]$  direction at different energies corresponding to those in Figs. 3 and 4, where the wave-vector integration ranges are  $0.9 < H < 1.1$  for the  $K$  cuts and  $-0.1 < K < 0.1$  for the  $H$  cuts. The solid lines are Gaussian fitting results for each doping and spin waves in the parent compound  $\text{BaFe}_2\text{As}_2$ .<sup>27</sup>

incommensurate on moving to  $x = 0.15, 0.18$ . For energies of  $E = 16 \pm 2$  [Fig. 6(c)],  $48 \pm 4$  [Fig. 6(d)], and  $60 \pm 10$  [Fig. 6(e)] meV, the electron-doping induced spin excitation intensity reduction becomes smaller. Finally, there are no significant difference between spin excitations of the parent compound and  $x = 0.096, 0.15, 0.18$  at  $E = 96 \pm 10$  [Fig. 6(f)],  $129 \pm 10$  [Fig. 6(g)],  $181 \pm 10$  [Fig. 6(h)], and  $225 \pm 10$  meV [Fig. 6(i)]. Figures 7(a)–7(d) show the comparison of  $[H, 0]$  scans for the  $x = 0.096, 0.15$ , and  $0.18$  samples at  $E = 16 \pm 2, 48 \pm 4, 96 \pm 10$ , and  $129 \pm 10$  meV. While the electron-doping evolution of the spin excitation intensity is consistent with cuts along the  $[1, K]$  direction, they are commensurate at all energies probed.

To illustrate further the electron-doping evolution of the spin excitations in the overdoped regime, we compare constant- $Q$  cuts in spin excitations of  $\text{BaFe}_{2-x}\text{Ni}_x\text{As}_2$  with  $x = 0, 0.096, 0.15$ , and  $0.18$  in Fig. 8.<sup>29</sup> The arrows in the inset of Fig. 8(a) show the directions of the constant- $Q$  cuts. At wave vectors near the Brillouin zone center at  $Q = (1, 0.05)$  and  $(1, 0.2)$ , electron-doping clearly suppresses the low-energy spin excitations. On increasing the wave vector to  $Q = (1, 0.35)$  and  $(1, 0.5)$ , there are much less difference in spin excitations of undoped and doped materials. Spin excitations form a broad peak near 100 meV in electron-overdoped samples similar to spin waves in parent compound.

Having established the electron-doping evolution of the overall spin excitations spectra, we now describe the effect of

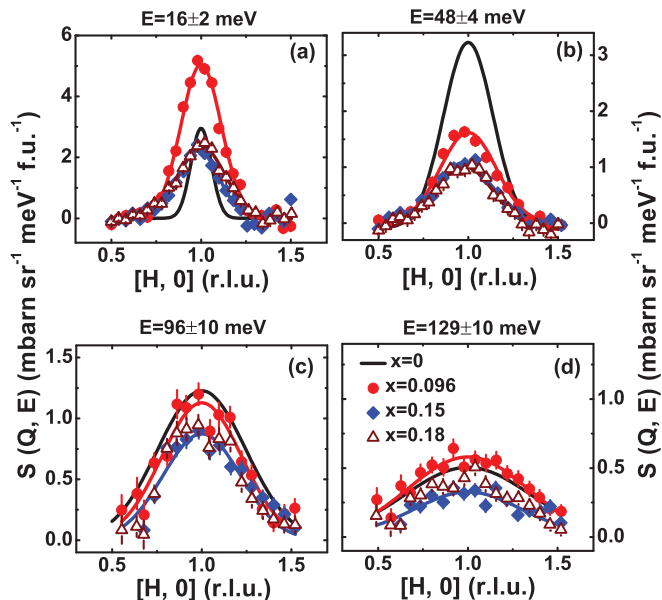


FIG. 7. (Color online) Constant-energy cuts of the spin excitations in  $\text{BaFe}_{2-x}\text{Ni}_x\text{As}_2$  along the  $[H, 0]$  direction at (a)  $E = 16 \pm 2$ , (b)  $48 \pm 4$ , (c)  $96 \pm 10$ , and (d)  $129 \pm 10$  meV. The solid lines are spin wave cuts in parent compound, and the reduced intensity compared with the doped material at  $E = 16 \pm 2$  meV is due to the presence of a large spin anisotropy gap.<sup>44</sup> The spin excitations are commensurate at all energies probed.

superconductivity on the low-energy spin excitations. From previous work, we know that a neutron spin resonance appears in the superconducting state of iron pnictides.<sup>15–26</sup> Careful temperature-dependent study of the resonance in the superconducting  $\text{BaFe}_{1.85}\text{Co}_{0.15}\text{As}_2$  iron pnictide suggests that the mode energy decreases on warming to  $T_c$  and is coupled with the decreasing superconducting gap energy.<sup>20</sup> This is different from the resonance in superconducting iron chalcogenide  $\text{Fe}_{1+\delta}\text{Te}_{1-x}\text{Se}_x$ , where the mode energy

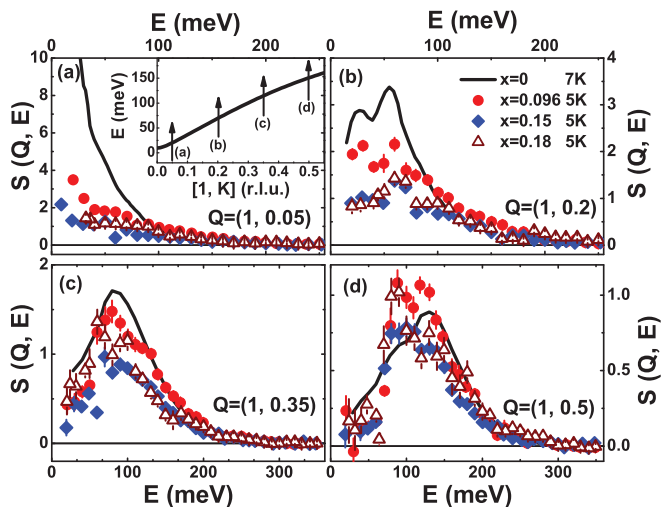


FIG. 8. (Color online) Constant- $Q$  cuts in the spin excitations of  $\text{BaFe}_{2-x}\text{Ni}_x\text{As}_2$  at wave vectors (a)  $Q = (1, 0.05)$ , (b)  $(1, 0.2)$ , (c)  $(1, 0.35)$ , and (d)  $(1, 0.5)$  as marked by the vertical arrows in the inset of (a). The solid lines are identical cuts from spin waves in  $\text{BaFe}_2\text{As}_2$ .<sup>27</sup>

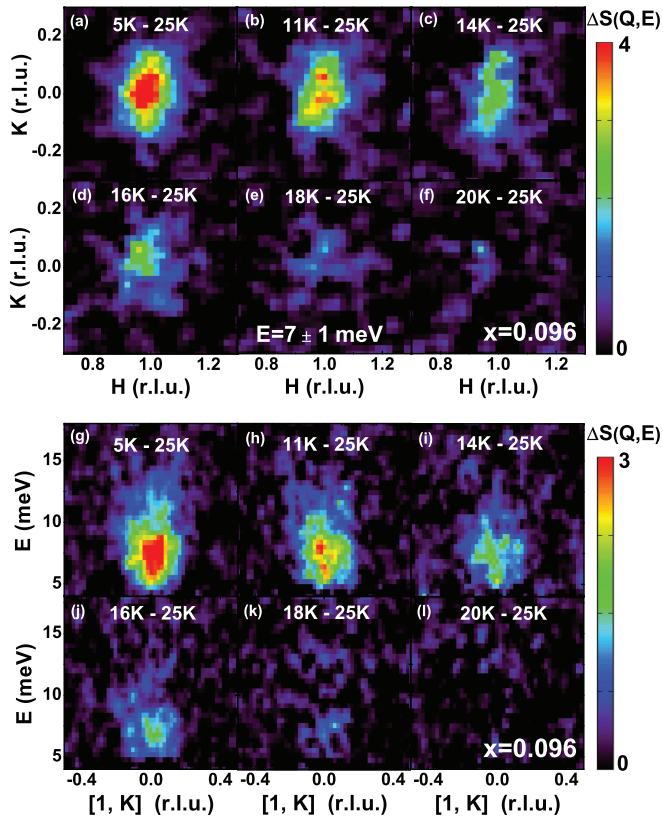


FIG. 9. (Color online) (a)–(f) The wave-vector dependence of the resonance in  $\text{BaFe}_{1.904}\text{Ni}_{0.096}\text{As}_2$  at  $T = 5, 11, 14, 16, 18,$  and  $20$  K after subtracting the normal state data at  $25$  K. (g)–(l) Energy dependence of the two-dimensional slices along the  $Q = [1, K]$  direction for the resonance at different temperatures. The mode essentially disappears around  $20$  K, but its peak positions are weakly temperature dependent.

is weakly temperature dependent.<sup>45–52</sup> Very recently, a sharp neutron spin resonance has been identified in superconducting  $\text{NaFe}_{0.935}\text{Co}_{0.045}\text{As}$  ( $T_c = 18$  K) iron pnictide.<sup>53</sup> Here, the resonance energy is again found to be weakly temperature dependent similar to the mode in  $\text{Fe}_{1+\delta}\text{Te}_{1-x}\text{Se}_x$ .<sup>53</sup> In order to probe the detailed temperature dependence of the resonance in  $\text{BaFe}_{1.904}\text{Ni}_{0.096}\text{As}_2$ , we carried out TOF INS measurements on MERLIN with  $E_i = 30$  meV at many temperatures below and above  $T_c$ . Following previous practice,<sup>15–26</sup> we used the  $T = 25$  K data as background and assumed that the net intensity gain near the AF ordering wave vector at lower temperatures is the resonance. Since an incident beam energy of  $E_i = 30$  meV corresponds to  $L \approx 1$  r.l.u. near the resonance energy of  $E_r \approx 7$  meV, we can simultaneously probe the wave vector and energy dependence of the mode below  $T_c$ . Figures 9(a)–9(f) show the wave-vector dependence of the temperature differences (the low-temperature data minus the data at  $25$  K) in spin excitations,  $S(\mathbf{Q}, E, T) - S(\mathbf{Q}, E, T = 25 \text{ K})$  with  $E_r = 7 \pm 1$  meV, at  $T = 5, 11, 14, 16, 18, 20$  K, respectively. At  $T = 5$  K, the superconductivity-induced resonance forms a transversely elongated ellipse in the  $[H, K]$  plane centered at  $\mathbf{Q}_{\text{AF}} = (1, 0)$  [Fig. 9(a)]. On warming to  $T = 11$  K [Fig. 9(b)],  $14$  K [Fig. 9(c)], and  $16$  K [Fig. 9(d)], the resonance becomes weaker and broader along both the

$[H, 0]$  and  $[1, K]$  directions. The resonance becomes almost indistinguishable from the background at  $T = 20$  K [Fig. 9(f)].

Figures 9(g)–9(l) show the net magnetic scattering above the  $T = 25$  K background projected onto the  $[1, K]$  and energy space at different temperatures. At  $T = 5$  K, we see a clear neutron spin resonance centered at  $E_r = 7 \pm 1$  meV and  $\mathbf{Q}_{\text{AF}} = (1, 0)$  [Fig. 9(g)]. Although the intensity of the resonance becomes progressively weaker on warming up to temperatures  $T = 11$  K [Fig. 9(h)],  $14$  K [Fig. 9(i)], and  $16$  K [Fig. 9(j)], its peak position in energy appears to be fixed at  $E \approx 7$  meV. On further warming to  $T = 18$  K [Fig. 9(k)], one can still see a weak resonance near  $E_r \approx 7$  meV. It becomes impossible to discern any magnetic signal at  $T = 20$  K above the  $T = 25$  K background scattering [Fig. 9(l)].

To quantitatively determine the temperature evolution of the resonance, we cut the images in Figs. 9(g)–9(l) along the energy direction by integrating wave vectors  $0.8 < H < 1.2$  and  $-0.2 < K < 0.2$  r.l.u. around  $\mathbf{Q}_{\text{AF}} = (1, 0)$ . Figure 10(a) shows the outcome at temperatures in Fig. 9(g)–9(l) and additional data taken at  $T = 19$  and  $22$  K. At all temperatures below  $T_c = 20$  K, we see a well-defined resonance showing as positive scattering above background near  $E = 7$  meV. There are no statistical differences in magnetic scattering for temperatures between  $T = 20, 22,$  and  $25$  K. Figure 10(b) shows the wave-vector cuts along the  $[1, K]$  direction with energy integration of  $E = 7 \pm 1$  meV and  $\mathbf{Q}$  integration from  $0.9 < H < 1.1$  at different temperatures. There are well-defined peaks centered at the commensurate AF ordering wave vector for all probed temperatures. The solid lines are Gaussian fits to the data, which give peak intensity and FWHM of the spin excitations. Figure 10(c) shows similar wave-vector cuts along the  $[H, 0]$  direction with Gaussian fits. The superconductivity-induced effects on wave-vector dependence of the resonance along the  $[1, K]$  and  $[H, 0]$  directions are shown in Figs. 10(d) and 10(e), respectively. The data are peaked around the  $\mathbf{Q}_{\text{AF}} = (1, 0)$  wave vector and the solid lines are Gaussian fits on zero backgrounds.

Using parameters obtained from fits to the spin excitations spectra in Fig. 10, we can determine the temperature dependence of the resonance energy, intensity, and  $\mathbf{Q}$  widths along the  $[1, K]$  and  $[H, 0]$  directions. These results can be compared with temperature dependence of the superconducting gaps determined from other methods.<sup>54–56</sup> From angle resolved photoemission spectroscopy experiments,<sup>54</sup> it is well known that the electron-doped  $\text{BaFe}_{2-x}\text{Te}_x\text{As}_2$  iron pnictides have the large isotropic superconducting gaps  $\Delta_h$  located on the hole Fermi surface near the zone center position  $\Gamma$  and the small gap  $\Delta_e$  on one of the electron Fermi surfaces near  $M$  point. The temperature dependence of the superconducting gaps decrease with increasing temperature and vanish at  $T_c$ . The pink solid line in Fig. 11(a) shows temperature dependence of the sum of the electron and hole Fermi surface superconducting gaps  $\Delta_e + \Delta_h$  obtained from point-contact Andreev reflection measurements on  $\text{BaFe}_{1.9}\text{Ni}_{0.1}\text{As}_2$ .<sup>56</sup> By comparing the temperature dependence of the resonance in the color contour plot and the solid points with the pink solid line, we see that the energy position of the resonance is weakly temperature dependent and does not follow the temperature dependence of the sum of the electron and hole pocket superconducting

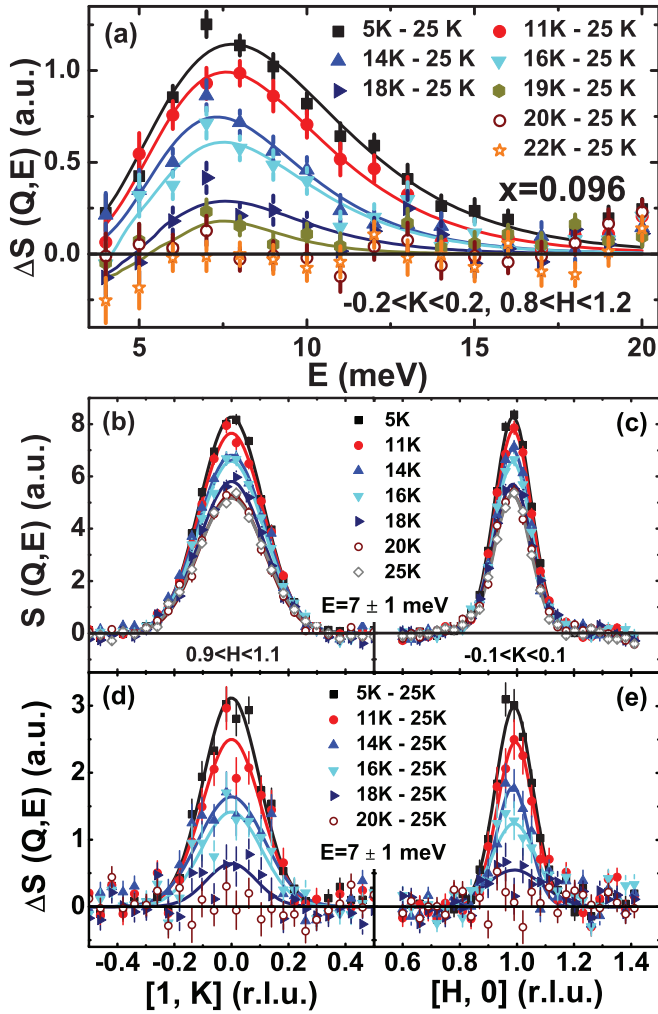


FIG. 10. (Color online) Temperature dependence of the resonance in  $\text{BaFe}_{1.904}\text{Ni}_{0.096}\text{As}_2$  measured with  $E_i = 20$  meV. (a) The difference of constant- $Q$  cuts between the low-energy spin excitations at  $T < 25$  K and normal state at  $T = 25$  K around AF ordering wave vector with integration range  $0.8 < H < 1.2$  and  $-0.2 < K < 0.2$ . (b) and (c) Constant-energy cuts along the  $Q = [1, K]$  and  $[H, 0]$  directions at different temperatures and  $E = 7 \pm 1$  meV. (d) and (e) Wave-vector dependence of the resonance at  $E = 7 \pm 1$  meV.

gaps. This is similar to the temperature dependence of the resonance in superconducting iron chalcogenide  $\text{Fe}_{1+\delta}\text{Te}_{1-x}\text{Se}_x$  (Refs. 46 and 52) and  $\text{NaFe}_{0.935}\text{Co}_{0.045}\text{As}$  iron pnictide.<sup>53</sup>

Figure 11(b) shows the temperature dependence of the wave-vector-integrated ( $0.8 < H < 1.2$  and  $-0.2 < K < 0.2$ ) magnetic spectral weight. Consistent with earlier measurements,<sup>30</sup> the spectral weight of the resonance increases below  $T_c$  like an order parameter of superconductivity. The filled solid circles in Figs. 11(c) and 11(d) plot temperature dependence of FWHM of the resonance along the transverse and longitudinal directions, respectively. The open circles in Fig. 11(c) show temperature dependence of the FWHM of the resonance obtained on TAIPAN triple-axis spectrometer. We see that the widths of the resonance display a clear superconductivity-induced narrowing below  $T_c$  along both the transverse and longitudinal directions. In the case of hole-doped iron pnictide superconductor  $\text{Ba}_{0.67}\text{K}_{0.33}\text{Fe}_2\text{As}_2$  ( $T_c =$

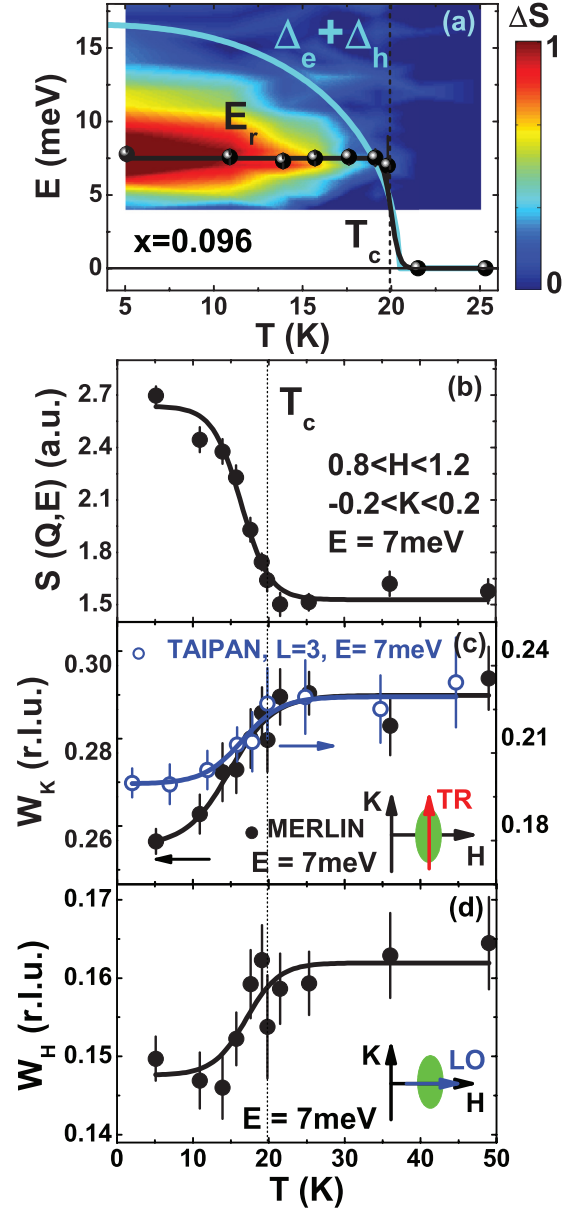


FIG. 11. (Color online) (a) Temperature dependence of the resonance energy  $E_r$  and the sum of superconducting gaps  $\Delta_e + \Delta_h$  for  $\text{BaFe}_{1.904}\text{Ni}_{0.096}\text{As}_2$ .<sup>56</sup> The color bars represent the intensity gain  $\Delta S(Q, E)$  around AF ordering wave vector in the superconducting state. (b) Temperature dependence of the integrated intensity of the spin excitations at  $E = 7$  meV with integration range  $0.8 < H < 1.2$  and  $-0.2 < K < 0.2$ . (c) and (d) Temperature dependence of FWHM (peak width) along the  $[1, K]$  ( $W_K$ ) and  $[H, 0]$  ( $W_H$ ) directions at  $E = 7$  meV. The blue open circles are the similar results from the triple-axis experiments at fixed  $L = 3$ .

38 K), the resonance at  $E_r = 15$  meV has a longitudinally elongated line shape around the AF ordering wave vector  $\mathbf{Q}_{\text{AF}} = (1, 0)$  in the superconducting state.<sup>57</sup> Upon warming across  $T_c$ , the resonance become isotropic circle in reciprocal space.<sup>33</sup> Such behavior is different from the resonance in electron-doped  $\text{BaFe}_{1.904}\text{Ni}_{0.096}\text{As}_2$  superconductor, where the transversely elongated spin excitations become slightly narrower below  $T_c$ . In a recent INS experiment on superconducting  $\text{BaFe}_{1.926}\text{Ni}_{0.074}\text{As}_2$  ( $T_c = 17$  K),<sup>32</sup> the resonance

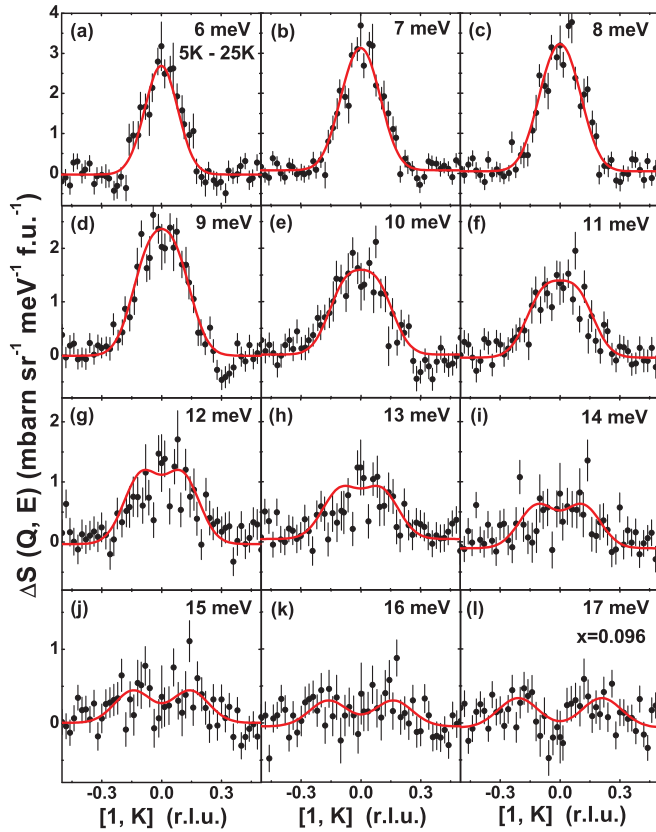


FIG. 12. (Color online) Wave-vector dependence of the resonance as a function of increasing energy for  $\text{BaFe}_{1.904}\text{Ni}_{0.096}\text{As}_2$ . Using the color plot in Fig. 9(g), we cut the data along the  $[1, K]$  direction for energies of (a)  $E = 6 \pm 1$ , (b)  $7 \pm 1$ , (c)  $8 \pm 1$ , (d)  $9 \pm 1$ , (e)  $10 \pm 1$ , (f)  $11 \pm 1$ , (g)  $12 \pm 1$ , (h)  $13 \pm 1$ , (i)  $14 \pm 1$ , (j)  $15 \pm 1$ , (k)  $16 \pm 1$ , and (l)  $17 \pm 1$  meV. The solid lines are fitting results by two symmetric Gaussian functions on flat backgrounds.

at  $E_r = 6$  meV was found to have spin-wave-like dispersion along the transverse direction. In our TOF INS measurements for  $\text{BaFe}_{1.904}\text{Ni}_{0.096}\text{As}_2$ , this would correspond to a dispersive resonance along the transverse  $[1, K]$  direction in Fig. 9(g). To see if we can detect the possible dispersion of the resonance, we cut the temperature difference plot in Fig. 9(g) along the  $[1, K]$  direction in 1 meV interval. The outcome in Fig. 12 shows that the resonance indeed disperses outward for energies above  $\sim 10$  meV along the transverse direction. This result, combined with earlier observation of incommensurate resonance in electron overdoped  $\text{BaFe}_{1.85}\text{Ni}_{0.15}\text{As}_2$ ,<sup>30</sup> indicate that the transversely dispersive resonance mode is prevalent in both the electron underdoped<sup>32</sup> and overdoped  $\text{BaFe}_{2-x}\text{Ni}_x\text{As}_2$ . At present, it is unclear how to understand the wave-vector narrowing of the resonance below  $T_c$  [Figs. 11(c) and 11(d)] at  $E = 7$  meV and the dispersion of the mode at higher energies from Fermi surface nesting point of view.<sup>30,58–60</sup>

Having described the temperature, wave vector, and energy dependence of the low-energy spin excitations in  $\text{BaFe}_{1.904}\text{Ni}_{0.096}\text{As}_2$ , we now discuss similar TOF INS measurements for  $\text{BaFe}_{1.85}\text{Ni}_{0.15}\text{As}_2$ . In previous triple-axis and TOF INS measurements on  $\text{BaFe}_{1.85}\text{Ni}_{0.15}\text{As}_2$ ,<sup>30</sup> an incommensurate neutron spin resonance has been identified. Figure 13(a) shows the temperature difference of spin

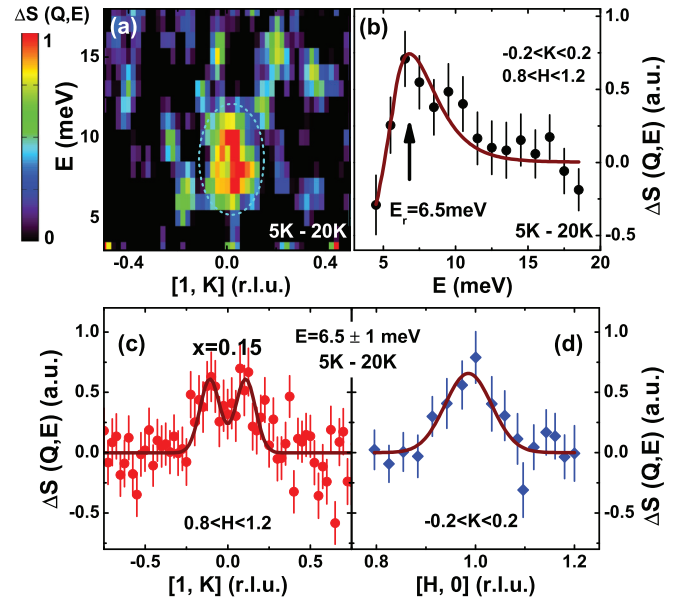


FIG. 13. (Color online) The temperature difference plot showing the presence of a resonance near  $E_r = 6.5$  meV projected onto the energy- $[1, K]$  plane for  $\text{BaFe}_{1.85}\text{Ni}_{0.15}\text{As}_2$ . The data were taken using  $E_i = 25$  meV with incident beam along the  $c$  axis. (a) The two-dimensional image of the spin excitations between  $T = 5$  and 20 K. (b) Intensity gain of the resonance obtained by integrating  $0.8 < H < 1.2$  and  $-0.2 < K < 0.2$ . The mode occurs at  $E_r = 6.5$  meV at 5 K. (c) Wave-vector dependence of the resonance showing incommensurability along the  $[1, K]$  direction. (d) The resonance is commensurate along the  $[H, 0]$  direction.

excitations between 5 and 20 K projected onto the energy and  $[1, K]$  plane. By integrating wave vectors from  $0.8 < H < 1.2$  and  $-0.2 < K < 0.2$ , we plot the energy dependence of the resonance in Fig. 13(b). The mode energy is now at  $E_r = 6.5$  meV compared with  $E_r = 7$  meV for  $\text{BaFe}_{1.904}\text{Ni}_{0.096}\text{As}_2$ . Figure 13(c) shows a wave-vector cut along the  $[1, K]$  direction at  $E = 6.5 \pm 1$  meV, which confirm the transverse incommensurate nature of the resonance. A similar cut along the  $[H, 0]$  direction indicates that the mode is commensurate along the longitudinal direction [Fig. 13(d)].

Turning our attention to a more electron overdoped sample  $\text{BaFe}_{1.82}\text{Ni}_{0.18}\text{As}_2$  with  $T_c = 8$  K, we were unable to find any magnetic signal in previous triple-axis measurements using 8 g of sample.<sup>30</sup> Using 25 g of co-aligned single crystals with an incident neutron beam energy of  $E_i = 20$  meV along the  $c$  axis, we can now detect clear low-energy spin excitations at the AF wave-vector positions on MERLIN. Figures 14(a) and 14(b) show spin excitation images projected onto the energy and  $[1, K]$  planes at  $T = T_c - 3 = 5$  K and  $T = T_c + 2 = 10$  K, respectively. Consistent with the behavior of spin excitations at other Ni-doping levels, we see plumes of scattering stemming from  $\mathbf{Q}_{\text{AF}} = (1, 0)$ . In the normal state (10 K), spin excitations are commensurate and centered at  $\mathbf{Q}_{\text{AF}} = (1, 0)$  from  $E = 4$  to 9 meV [Fig. 14(b)]. On cooling to below  $T_c$  (5 K), the scattering is enhanced between  $E = 5$  and 7 meV [Fig. 14(a)]. The temperature difference plot in Fig. 14(c) reveals evidence for incommensurate spin excitations.

Figures 14(d) and 14(e) show wave-vector dependence of the spin excitations in the  $[H, K]$  plane at the resonance

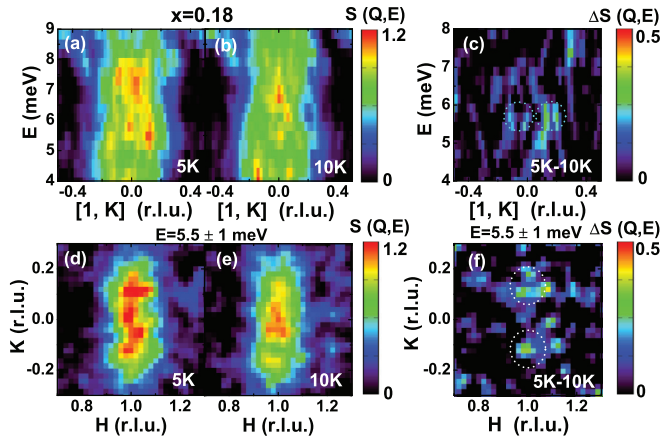


FIG. 14. (Color online) Temperature dependence of the spin excitations in  $\text{BaFe}_{1.82}\text{Ni}_{0.18}\text{As}_2$  measured with  $E_r = 20$  meV. (a)–(c) Energy dependence of the two-dimensional slices along the  $Q = [1, K]$  direction at  $T = 5$  K, 10 K, and their differences, respectively. (d)–(f) Wave-vector dependence of the two-dimensional slices in the energy range  $E = 5.5 \pm 1$  meV at 5- and 10 K, and their difference, respectively. The dashed circles mark positions of incommensurate spin fluctuations.

energy  $E_r = 5.5 \pm 1$  meV below and above  $T_c$ , respectively. In the normal state (10 K), spin excitations form transversely elongated ellipse commensurate with the underlying lattice [Fig. 14(e)]. On cooling to below  $T_c$  (5 K), spin excitations at transversely incommensurate positions are enhanced [Fig. 14(d)]. The temperature differences between 5 and 10 K reveal transversely incommensurate spin excitations marked by dashed circles [Fig. 14(f)].

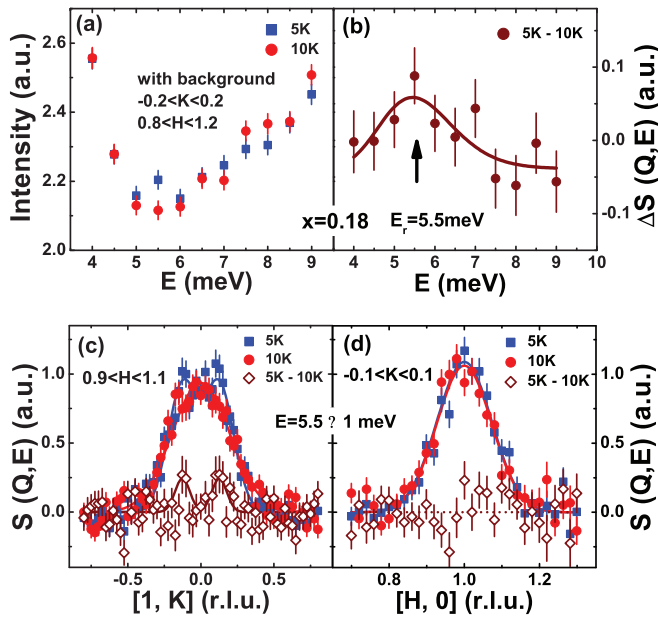


FIG. 15. (Color online) (a) and (b) Energy dependence of the low-energy spin excitations in  $\text{BaFe}_{1.82}\text{Ni}_{0.18}\text{As}_2$  at 5 and 10 K, and their difference. (c), (d) Wave-vector dependence of the low-energy spin excitations in the energy range  $E = 5.5 \pm 1$  meV at 5 and 10 K, and their difference.

To further probe the wave vector, energy, and temperature dependence of the magnetic excitations in  $\text{BaFe}_{1.82}\text{Ni}_{0.18}\text{As}_2$ , we show in Fig. 15(a) the energy dependence of the spin excitations near the AF ordering position integrated within the range of  $-0.2 < K < 0.2$  and  $0.8 < H < 1.2$  r.l.u. below and above  $T_c$ . The data reveal a small enhancement of the scattering below  $T_c$  for energies around  $E_r = 5.5$  meV. Figure 15(b) shows the temperature difference between 5 and 10 K, and one can see a very weak resonance near  $E_r = 5.5$  meV. Figure 15(c) shows cuts along the  $[1, K]$  direction at  $E = 5.5 \pm 1$  meV and  $0.9 < H < 1.1$ . The red circles are data at 10 K showing a commensurate peak centered at  $\mathbf{Q}_{\text{AF}} = (1, 0)$ . The blue squares are identical cut at 5 K, which have more scattering at the incommensurate positions. The brown diamonds are the temperature difference plot, which again reveal the incommensurate neutron spin resonance. Figure 15(d) shows similar cuts along the  $[H, 0]$  direction. The scattering peaks at the commensurate AF ordering position and has no observable changes across  $T_c$ , as confirmed by the temperature difference plot shown as brown diamonds in Fig. 15(d). Therefore the resonance in electron-overdoped  $\text{BaFe}_{1.82}\text{Ni}_{0.18}\text{As}_2$  arises entirely from superconductivity-induced incommensurate spin excitations.

In previous work,<sup>29,33</sup> we have established the electron doping evolution of the local dynamic susceptibility  $\chi''(E)$  for  $\text{BaFe}_{2-x}\text{Ni}_x\text{As}_2$  with  $x = 0, 0.1, 0.3$ . The new result serves to fill in the gap between the optimally electron-doped superconductor and electron-overdoped nonsuperconductor. Figure 16(a) shows the comparison of the energy dependent  $\chi''(E)$  for  $x = 0, 0.096, 0.15$  and  $0.18$ , using method described before.<sup>29,33</sup> The solid line is the result for  $\text{BaFe}_2\text{As}_2$ .<sup>29</sup> The energy dependence of the local susceptibility for  $\text{BaFe}_{1.904}\text{Ni}_{0.096}\text{As}_2$  is almost identical to that of  $\text{BaFe}_{1.9}\text{Ni}_{0.1}\text{As}_2$ .<sup>29</sup> On increasing the electron doping levels to  $x = 0.15$  and  $0.18$ , we see a significant suppression of the local dynamic susceptibility for energies below  $\sim 80$  meV. Instead of forming clear peak at the resonance energy as in the case of  $\text{BaFe}_{1.904}\text{Ni}_{0.096}\text{As}_2$ , the energy dependent  $\chi''(E)$  increases linearly with increasing energy and the superconductivity-induced resonance is not a visible peak in  $\text{BaFe}_{2-x}\text{Ni}_x\text{As}_2$  with  $x = 0.15$  and  $0.18$  [Fig. 16(a)]. For spin excitation energies above  $\sim 80$  meV, electron-doping to  $\text{BaFe}_2\text{As}_2$  appears to have little effect on the local dynamic susceptibility. These results are consistent with the notion that Fermi surface nesting and itinerant electrons are controlling the low-energy spin excitations while high-energy spin excitations arise from the local moments.<sup>4,61–64</sup> Upon further doping to electron-overdoped nonsuperconductor for  $\text{BaFe}_{2-x}\text{Ni}_x\text{As}_2$  with  $x > 0.25$ , Fermi surface nesting between the hole Fermi surface near  $\Gamma$  and electron Fermi surface near  $M$  point breaks down,<sup>65</sup> together with vanishing superconductivity and low-energy spin excitations.<sup>28,41</sup> However, high-energy spin excitations associated with local moments are not affected.<sup>33</sup> At present, it is unclear whether the large spin gap of  $\sim 50$  meV in  $\text{BaFe}_{1.7}\text{Ni}_{0.3}\text{As}_2$  (Ref. 33) opens gradually or suddenly upon entering into the nonsuperconducting state with increasing electron doping  $x$ . Future work in this area might shed light on the relationship between the low-energy spin excitations and Fermi surface nesting.

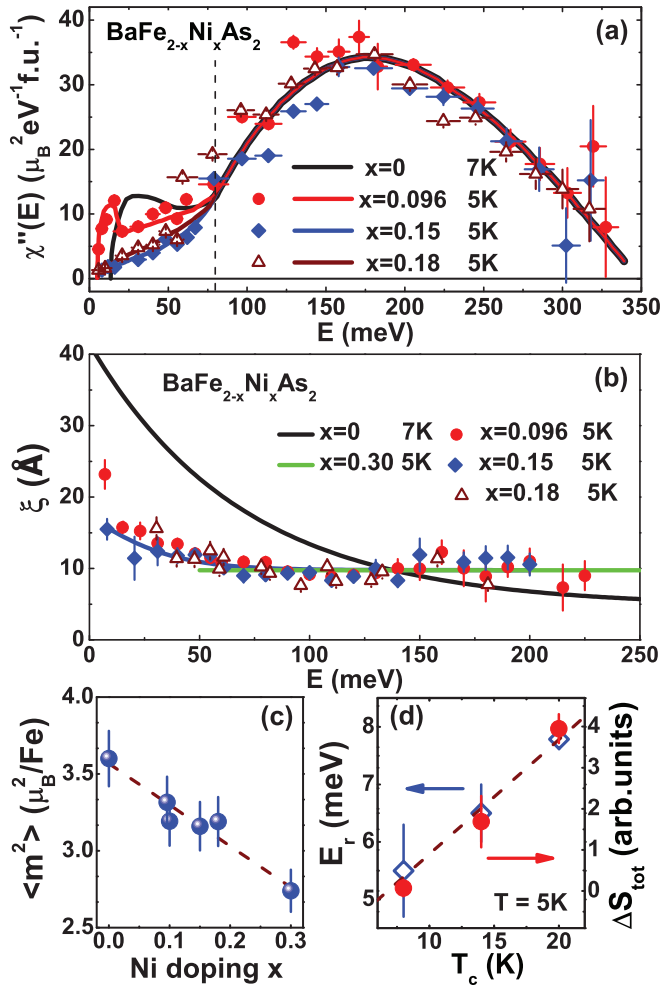


FIG. 16. (Color online) (a) Energy dependence of the local dynamic susceptibility  $\chi''(E)$  for  $\text{BaFe}_{2-x}\text{Ni}_x\text{As}_2$  with  $x = 0, 0.096, 0.15, 0.18$  in the absolute units ( $\mu_B^2/\text{eV}/\text{f.u.}^{-1}$ ). While the high-energy spin excitations are doping independent, low-energy spin excitations ( $E < 80$  meV) decrease with increasing electron doping. (b) Energy dependence of the dynamic spin-spin correlation lengths ( $\xi$ ) for  $\text{BaFe}_{2-x}\text{Ni}_x\text{As}_2$  with  $x = 0, 0.096, 0.15, 0.18, 0.30$  obtained by Fourier transform of the constant-energy cuts along the  $[1, K]$  direction. (c) Ni-doping dependence of the total fluctuating moment. (d) The  $T_c$  dependence of the resonance energy and its spectral weight.

Figure 16(b) shows the electron doping dependence of the dynamic spin-spin correlation lengths, obtained by Fourier transform of the  $Q = [1, K]$  dependence of the spin dynamic susceptibility.<sup>29</sup> As we can see from the Figure, electron doping from an optimally doped superconductor to electron-overdoped superconductor only appears to shorten the spin-spin correlation length for spin excitations at low energies, and have little impact to the zone boundary spin excitations. To understand the impact of electron doping to the total fluctuating magnetic moments, defined as  $\langle m^2 \rangle = (3/\pi) \int \chi''(E) dE / [1 - \exp(-E/k_B T)]$ ,<sup>22</sup> we show in Fig. 16(c) the electron-doping dependence of  $\langle m^2 \rangle$  for  $\text{BaFe}_{2-x}\text{Ni}_x\text{As}_2$  with  $x = 0, 0.096, 0.1, 0.15, 0.18, 0.3$ .<sup>29,33,43</sup> We used  $\langle m^2 \rangle \approx 3.6 \mu_B^2/\text{Fe}$  for  $\text{BaFe}_2\text{As}_2$  from a recent work,<sup>43</sup> a value slightly larger than the earlier estimation of  $\langle m^2 \rangle \approx 3.17 \pm 0.16 \mu_B^2/\text{Fe}$ .<sup>29</sup> The  $\langle m^2 \rangle$  shows a linear

decrease in value with increasing  $x$ . From the electron doping dependence of the local dynamic susceptibility  $\chi''(E)$  in Fig. 16(a), we see that the decreasing total moment ( $m^2$ ) with increasing  $x$  in  $\text{BaFe}_{2-x}\text{Ni}_x\text{As}_2$  is due almost entirely to the reduction in spin excitations below  $\sim 80$  meV.

Finally, Fig. 16(d) shows the total spectral weight of spin resonance and the energy positions at  $T = 5$  K, estimated from the superconductivity-induced spin excitation change, as a function of  $T_c$ . The resonance energy is linearly scaling with  $T_c$ , the same as previous results in cuprates and pnictides.<sup>21,23,66</sup> As superconductivity ceases to exist for  $\text{BaFe}_{2-x}\text{Ni}_x\text{As}_2$  with  $x \rightarrow 0.25$ , superconductivity-induced low-energy resonance also approaches zero, even though the high-energy spin excitations are not much affected. This is consistent with the notion that superconductivity requires itinerant electron-spin excitation coupling,<sup>33</sup> and the Fermi surface nesting driven low-energy spin excitations are important for superconductivity in electron-doped iron pnictides.

#### IV. DISCUSSION AND CONCLUSIONS

By comparing the structure, phase diagram, and magnetic excitations in high- $T_c$  copper oxide, iron-based, and heavy fermion superconductors, Scalapino concludes that spin fluctuation-mediated pairing is the common thread linking different classes unconventional superconductors.<sup>2</sup> Within the framework of this picture, the superconducting condensation energy should be accounted for by the change in magnetic exchange energy  $\Delta E_{\text{ex}}(T)$  between the normal ( $N$ ) and superconducting ( $S$ ) phases at zero temperature. For an isotropic  $t$ - $J$  model,  $\Delta E_{\text{ex}}(T) = 2J[\langle \mathbf{S}_{i+x} \cdot \mathbf{S}_i \rangle_N - \langle \mathbf{S}_{i+x} \cdot \mathbf{S}_i \rangle_S]$ , where  $J$  is the nearest-neighbor magnetic exchange coupling and  $\langle \mathbf{S}_{i+x} \cdot \mathbf{S}_i \rangle$  is the magnetic scattering in absolute units at temperature  $T$ .<sup>2</sup> If there are no changes in magnetic scattering between the normal and superconducting states, spin excitations should not contribute to the superconducting condensation energy. This is consistent with the observation that superconductivity-induced effect in spin excitations becomes very weaker in electron-overdoped iron pnictides with reduced  $T_c$ . While the total fluctuating moment  $\langle m^2 \rangle$  only decreases slightly on moving from the AF parent compound  $\text{BaFe}_2\text{As}_2$  to electron-overdoped nonsuperconducting  $\text{BaFe}_{1.7}\text{Ni}_{0.3}\text{As}_2$  [Fig. 16(c)], the changes in resonance intensity appears to correlate with superconducting  $T_c$  [Fig. 16(d)]. This suggests that the superconducting transition temperature in electron-doped iron pnictides is associated with the strength of the itinerant electron-low-energy spin excitations coupling or Fermi surface nesting conditions of the hole and electron pockets. This is not to say that high-energy spin excitations associated with local moments are not important for superconductivity, as high-energy spin excitations provide the basis for having a large effective magnetic exchange coupling  $J$ , which is crucial for high- $T_c$  superconductivity.<sup>33</sup>

In conclusion, we use Triple-axis and TOF INS to study the temperature and electron-doping evolution of the spin excitations in  $\text{BaFe}_{2-x}\text{Ni}_x\text{As}_2$  with  $x = 0.096, 0.15, 0.18$ . Whereas the low-energy resonance induced by superconductivity becomes weak and vanishes near the electron doping level when superconductivity ceases to exit, high-energy spin excitations

are hardly modified by electron-doping and superconductivity. For samples near optimal superconductivity, the FWHM of the resonance narrows in response to superconductivity. We establish the dispersion of the resonance for  $x = 0.096$  sample near optimal superconductivity, and show that incommensurate spin excitations are prevalent in both the electron underdoped and overdoped superconductors. Although the total magnetic fluctuating moment only decreases slightly with increasing electron doping, the low-energy spin excitations coupling with itinerant electrons vanishes when superconductivity is suppressed. These results suggest that the Fermi surface nesting and low-energy spin excitation-itinerant

electron coupling are critical for superconductivity in these materials.

#### ACKNOWLEDGMENTS

The work at the Institute of Physics, Chinese Academy of Sciences, is supported by the National Basic Research Program of China (Nos. 2011CBA00110 and 2012CB821400) and the National Science Foundation of China. The work at Rice University is supported by the U.S. National Science Foundation through Grants NSF-DMR-1063866 and NSF-OISE-0968226.

\*These authors made equal contributions to this paper.

†pdai@rice.edu

- <sup>1</sup>P. A. Lee, N. Nagaosa, and X.-G. Wen, *Rev. Mod. Phys.* **78**, 17 (2006).
- <sup>2</sup>D. J. Scalapino, *Rev. Mod. Phys.* **84**, 1383 (2012).
- <sup>3</sup>M. Fujita, H. Hiraka, M. Matsuda, M. Matsuura, J. M. Tranquada, S. Wakimoto, G. Xu, and K. Yamada, *J. Phys. Soc. Jpn.* **81**, 011007 (2012).
- <sup>4</sup>P. C. Dai, J. Hu, and E. Dagotto, *Nat. Phys.* **8**, 709 (2012).
- <sup>5</sup>J. M. Tranquada, G. Xu, and I. A. Zaliznyak, *J. Magn. Magn. Mater.* **350**, 148 (2014).
- <sup>6</sup>M. P. M. Dean, G. Dellea, R. S. Springell, F. Yakhov-Harris, K. Kummer, N. B. Brookes, X. Liu, Y. Sun, J. Strle, T. Schmitt, L. Braicovich, G. Ghiringhelli, I. Božović and J. P. Hill, *Nat. Mater.*, doi: [10.1038/nmat3723](https://doi.org/10.1038/nmat3723).
- <sup>7</sup>M. Le Tacon, M. Minola, D. C. Peets, M. Moretti Sala, S. Blanco-Canosa, V. Hinkov, R. Liang, D. A. Bonn, W. N. Hardy, C. T. Lin, T. Schmitt, L. Braicovich, G. Ghiringhelli, and B. Keimer, *Phys. Rev. B* **88**, 020501(R) (2013).
- <sup>8</sup>Y. Kamihara, T. Watanabe, M. Hirano, and H. Hosono, *J. Am. Chem. Soc.* **130**, 3296 (2008).
- <sup>9</sup>M. Rotter, M. Tegel, and D. Johrendt, *Phys. Rev. Lett.* **101**, 107006 (2008).
- <sup>10</sup>A. S. Sefat, R. Jin, M. A. McGuire, B. C. Sales, D. J. Singh, and D. Mandrus, *Phys. Rev. Lett.* **101**, 117004 (2008).
- <sup>11</sup>L. Li, Y. Luo, Q. Wang, H. Chen, Z. Ren, Q. Tao, Y. Li, X. Lin, M. He, Z. Zhu, G. Cao, and Z. Xu, *New J. Phys.* **11**, 025008 (2009).
- <sup>12</sup>C. de la Cruz, Q. Huang, J. W. Lynn, J. Li, W. Ratchiff II, J. L. Zarestky, H. A. Mook, G. Chen, J. Luo, N. Wang, and P. C. Dai, *Nature (London)* **453**, 899 (2008).
- <sup>13</sup>J. Zhao, Q. Huang, C. de la Cruz, S. Li, J. W. Lynn, Y. Chen, M. A. Green, G. Chen, G. Li, Z. Li, J. Luo, N. Wang, and P. C. Dai, *Nat. Mater.* **7**, 953 (2008).
- <sup>14</sup>Q. Huang, Y. Qiu, W. Bao, M. A. Green, J. W. Lynn, Y. C. Gasparovic, T. Wu, G. Wu, and X. H. Chen, *Phys. Rev. Lett.* **101**, 257003 (2008).
- <sup>15</sup>M. D. Lumsden, A. D. Christianson, D. Parshall, M. B. Stone, S. E. Nagler, G. J. MacDougall, H. A. Mook, K. Lokshin, T. Egami, D. L. Abernathy, E. A. Goremychkin, R. Osborn, M. A. McGuire, A. S. Sefat, R. Jin, B. C. Sales, and D. Mandrus, *Phys. Rev. Lett.* **102**, 107005 (2009).
- <sup>16</sup>S. Chi, A. Schneidewind, J. Zhao, L. W. Harriger, L. Li, Y. Luo, G. Cao, Z. Xu, M. Loewenhaupt, J. Hu, and P. C. Dai, *Phys. Rev. Lett.* **102**, 107006 (2009).

- <sup>17</sup>S. Li, Y. Chen, S. Chang, J. W. Lynn, L. Li, Y. Luo, G. Cao, Z. Xu, and P. C. Dai, *Phys. Rev. B* **79**, 174527 (2009).
- <sup>18</sup>D. K. Pratt, W. Tian, A. Kreyssig, J. L. Zarestky, S. Nandi, N. Ni, S. L. Bud'ko, P. C. Canfield, A. I. Goldman, and R. J. McQueeney, *Phys. Rev. Lett.* **103**, 087001 (2009).
- <sup>19</sup>A. D. Christianson, M. D. Lumsden, S. E. Nagler, G. J. MacDougall, M. A. McGuire, A. S. Sefat, R. Jin, B. C. Sales, and D. Mandrus, *Phys. Rev. Lett.* **103**, 087002 (2009).
- <sup>20</sup>D. S. Inosov, J. T. Park, P. Bourges, D. Sun, Y. Sidis, A. Schneidewind, K. Hradil, D. Haug, C. Lin, B. Keimer, and V. Hinkov, *Nat. Phys.* **6**, 178 (2010).
- <sup>21</sup>M. Wang, H. Luo, J. Zhao, C. Zhang, M. Wang, K. Marty, S. Chi, J. W. Lynn, A. Schneidewind, S. Li, and P. C. Dai, *Phys. Rev. B* **81**, 174524 (2010).
- <sup>22</sup>C. Lester, J.-H. Chu, J. G. Analytis, T. G. Perring, I. R. Fisher, and S. M. Hayden, *Phys. Rev. B* **81**, 064505 (2010).
- <sup>23</sup>J. T. Park, D. S. Inosov, A. Yaresko, S. Graser, D. L. Sun, Ph. Bourges, Y. Sidis, Y. Li, J.-H. Kim, D. Haug, A. Ivanov, K. Hradil, A. Schneidewind, P. Link, E. Faulhaber, I. Glavatsky, C. Lin, B. Keimer, and V. Hinkov, *Phys. Rev. B* **82**, 134503 (2010).
- <sup>24</sup>H. F. Li, C. Broholm, D. Vaknin, R. M. Fernandes, D. L. Abernathy, M. B. Stone, D. K. Pratt, W. Tian, Y. Qiu, N. Ni, S. O. Diallo, J. L. Zarestky, S. L. Bud'ko, P. C. Canfield, and R. J. McQueeney, *Phys. Rev. B* **82**, 140503(R) (2010).
- <sup>25</sup>D. S. Inosov, J. T. Park, A. Charnukha, Y. Li, A. V. Boris, B. Keimer, and V. Hinkov, *Phys. Rev. B* **83**, 214520 (2011).
- <sup>26</sup>M. Wang, H. Luo, M. Wang, S. Chi, J. A. Rodriguez-Rivera, D. Singh, S. Chang, J. W. Lynn, and P. C. Dai, *Phys. Rev. B* **83**, 094516 (2011).
- <sup>27</sup>L. W. Harriger, H. Q. Luo, M. C. Liu, C. Frost, J. P. Hu, M. R. Norman, and P. C. Dai, *Phys. Rev. B* **84**, 054544 (2011).
- <sup>28</sup>K. Matan, S. Ibuka, R. Morinaga, S. Chi, J. W. Lynn, A. D. Christianson, M. D. Lumsden, and T. J. Sato, *Phys. Rev. B* **82**, 054515 (2010).
- <sup>29</sup>M. Liu, L. W. Harriger, H. Luo, M. Wang, R. A. Ewings, T. Guidi, H. Park, K. Haule, G. Kotliar, S. M. Hayden, and P. C. Dai, *Nat. Phys.* **8**, 376 (2012).
- <sup>30</sup>H. Luo, Z. Yamani, Y. Chen, X. Lu, M. Wang, S. Li, T. A. Maier, S. Danilkin, D. T. Adroja, and P. C. Dai, *Phys. Rev. B* **86**, 024508 (2012).
- <sup>31</sup>G. S. Tucker, R. M. Fernandes, H.-F. Li, V. Thampy, N. Ni, D. L. Abernathy, S. L. Bud'ko, P. C. Canfield, D. Vaknin, J. Schmalian, and R. J. McQueeney, *Phys. Rev. B* **86**, 024505 (2012).
- <sup>32</sup>M. G. Kim, G. S. Tucker, D. K. Pratt, S. Ran, A. Thaler, A. D. Christianson, K. Marty, S. Calder, A. Podlesnyak, S. L. Bud'ko,

- P. C. Canfield, A. Kreyssig, A. I. Goldman, and R. J. McQueeney, *Phys. Rev. Lett.* **110**, 177002 (2013).
- <sup>33</sup>M. Wang, C. Zhang, X. Lu, G. Tan, H. Luo, Y. Song, M. Wang, X. Zhang, E. A. Goremychkin, T. G. Perring, T. A. Maier, Z. Yin, K. Haule, G. Kotliar, and P. C. Dai, [arXiv:1303.7339](https://arxiv.org/abs/1303.7339).
- <sup>34</sup>H. Luo, R. Zhang, M. Laver, Z. Yamani, M. Wang, X. Lu, M. Wang, Y. Chen, S. Li, S. Chang, J. W. Lynn, and P. C. Dai, *Phys. Rev. Lett.* **108**, 247002 (2012).
- <sup>35</sup>X. Lu, H. Gretarsson, R. Zhang, X. Liu, H. Luo, W. Tian, M. Laver, Z. Yamani, Y.-J. Kim, A. H. Nevidomskyy, Q. Si, and P. C. Dai, *Phys. Rev. Lett.* **110**, 257001 (2013).
- <sup>36</sup>I. I. Mazin, *Nature (London)* **464**, 183 (2010).
- <sup>37</sup>P. J. Hirschfeld, M. M. Korshunov, and I. I. Mazin, *Rep. Prog. Phys.* **74**, 124508 (2011).
- <sup>38</sup>A. V. Chubukov, *Annu. Rev. Condens. Matter Phys.* **3**, 57 (2012).
- <sup>39</sup>K. Kuroki, S. Onari, R. Arita, H. Usui, Y. Tanaka, H. Kontani, and H. Aoki, *Phys. Rev. Lett.* **101**, 087004 (2008).
- <sup>40</sup>F. Wang and D.-H. Lee, *Science* **332**, 200 (2011).
- <sup>41</sup>F. L. Ning, K. Ahilan, T. Imai, A. S. Sefat, M. A. McGuire, B. C. Sales, D. Mandrus, P. Cheng, B. Shen, and H.-H. Wen, *Phys. Rev. Lett.* **104**, 037001 (2010).
- <sup>42</sup>Y. Chen, X. Lu, M. Wang, H. Luo, and S. Li, *Supercond. Sci. Technol.* **24**, 065004 (2011).
- <sup>43</sup>L. W. Harriger, M. Liu, H. Luo, R. A. Ewings, C. D. Frost, T. G. Perring, and P. C. Dai, *Phys. Rev. B* **86**, 140403(R) (2012).
- <sup>44</sup>J. T. Park, G. Friemel, T. Loew, V. Hinkov, Y. Li, B. H. Min, D. L. Sun, A. Ivanov, A. Piovano, C. T. Lin, B. Keimer, Y. S. Kwon, and D. S. Inosov, *Phys. Rev. B* **86**, 024437 (2012).
- <sup>45</sup>H. A. Mook, M. D. Lumsden, A. D. Christianson, S. E. Nagler, B. C. Sales, R. Jin, M. A. McGuire, A. S. Sefat, D. Mandrus, T. Egami, and C. dela Cruz, *Phys. Rev. Lett.* **104**, 187002 (2010).
- <sup>46</sup>Y. Qiu, W. Bao, Y. Zhao, C. Broholm, V. Stanev, Z. Tesanovic, Y. C. Gasparovic, S. Chang, J. Hu, B. Qian, M. Fang, and Z. Mao, *Phys. Rev. Lett.* **103**, 067008 (2009).
- <sup>47</sup>M. D. Lumsden, A. D. Christianson, E. A. Goremychkin, S. E. Nagler, H. A. Mook, M. B. Stone, D. L. Abernathy, T. Guidi, G. J. MacDougall, C. de la Cruz, A. S. Sefat, M. A. McGuire, B. C. Sales, and D. Mandrus, *Nat. Phys.* **6**, 182 (2010).
- <sup>48</sup>S. H. Lee, G. Xu, W. Ku, J. S. Wen, C. C. Lee, N. Katayama, Z. J. Xu, S. Ji, Z. W. Lin, G. D. Gu, H. B. Yang, P. D. Johnson, Z. H. Pan, T. Valla, M. Fujita, T. J. Sato, S. Chang, K. Yamada, and J. M. Tranquada, *Phys. Rev. B* **81**, 220502 (2010).
- <sup>49</sup>D. N. Argyriou, A. Hiess, A. Akbari, I. Eremin, M. M. Korshunov, J. Hu, B. Qian, Z. Mao, Y. Qiu, C. Broholm, and W. Bao, *Phys. Rev. B* **81**, 220503 (2010).
- <sup>50</sup>S. Li, C. Zhang, M. Wang, H. Q. Luo, X. Lu, E. Faulhaber, A. Schneidewind, P. Link, J. Hu, T. Xiang, and P. C. Dai, *Phys. Rev. Lett.* **105**, 157002 (2010).
- <sup>51</sup>Z. Xu, J. Wen, G. Xu, Q. Jie, Z. Lin, Q. Li, S. Chi, D. K. Singh, G. Gu, and J. M. Tranquada, *Phys. Rev. B* **82**, 104525 (2010).
- <sup>52</sup>L. W. Harriger, O. J. Lipscombe, C. Zhang, H. Luo, M. Wang, K. Marty, M. D. Lumsden, and P. C. Dai, *Phys. Rev. B* **85**, 054511 (2012).
- <sup>53</sup>C. Zhang, H. F. Li, Y. Song, Y. Su, G. Tan, T. Netherton, C. Redding, S. V. Carr, O. Sobolev, A. Schneidewind, E. Faulhaber, L. W. Harriger, S. Li, X. Lu, D. X. Yao, T. Das, A. V. Balatsky, Th. Brückel, J. W. Lynn, and P. C. Dai, *Phys. Rev. B* **88**, 064504 (2013).
- <sup>54</sup>K. Terashimaa, Y. Sekiba, J. H. Bowen, K. Nakayama, T. Kawaharab, T. Sato, P. Richard, Y. Xu, L. Li, G. Cao, Z. Xu, H. Ding, and T. Takahashi, *Proc. Natl. Acad. Sci. USA* **106**, 7330 (2009).
- <sup>55</sup>M. A. Tanatar, J.-Ph. Reid, H. Shakeripour, X. G. Luo, N. Doiron-Leyraud, N. Ni, S. L. Bud'ko, P. C. Canfield, R. Prozorov, and L. Taillefer, *Phys. Rev. Lett.* **104**, 067002 (2010).
- <sup>56</sup>Z.-S. Wang, Z.-Y. Wang, H.-Q. Luo, X.-Y. Lu, J. Zhu, C.-H. Li, L. Shan, H. Yang, H.-H. Wen, and C. Ren, *Phys. Rev. B* **86**, 060508(R) (2012).
- <sup>57</sup>C. Zhang, M. Wang, H. Luo, M. Wang, M. Liu, J. Zhao, D. L. Abernathy, T. A. Maier, K. Marty, M. D. Lumsden, S. Chi, S. Chang, J. A. Rodriguez-Rivera, J. W. Lynn, T. Xiang, J. Hu, and P. C. Dai, *Sci. Rep.* **1**, 115 (2011).
- <sup>58</sup>T. A. Maier and D. J. Scalapino, *Phys. Rev. B* **78**, 020514(R) (2008).
- <sup>59</sup>T. A. Maier, S. Graser, D. J. Scalapino, and P. Hirschfeld, *Phys. Rev. B* **79**, 134520 (2009).
- <sup>60</sup>M. M. Korshunov and I. Eremin, *Phys. Rev. B* **78**, 140509(R) (2008).
- <sup>61</sup>K. Haule, J. H. Shim, and G. Kotliar, *Phys. Rev. Lett.* **100**, 226402 (2008).
- <sup>62</sup>Q. Si and E. Abrahams, *Phys. Rev. Lett.* **101**, 076401 (2008).
- <sup>63</sup>C. Fang, H. Yao, W.-F. Tsai, J. P. Hu, and S. A. Kivelson, *Phys. Rev. B* **77**, 224509 (2008).
- <sup>64</sup>C. Xu, M. Müller, and S. Sachdev, *Phys. Rev. B* **78**, 020501(R) (2008).
- <sup>65</sup>P. Richard, T. Sato, K. Nakayama, T. Takahashi, and H. Ding, *Rep. Prog. Phys.* **74**, 124512 (2011).
- <sup>66</sup>S. Li and P. C. Dai, *Front. Phys.* **6**, 429 (2011) (<http://link.springer.com/article/10.1107/s11467-011-0221-0>).